Supporting Information

Protein side-chain dynamics observed by solution- and solid-state NMR: comparative analysis of methyl ^{2}H relaxation data.

Bernd Reif[†]*, Yi Xue[‡], Vipin Agarwal[†], Maria S. Pavlova[‡], Maggy Hologne[†], Anne Diehl[†], Yaroslav E. Ryabov[‡], Nikolai R. Skrynnikov[‡]*

† *Forschunginstitut für Molekulare Pharmakologie (FMP), Robert-Rössle-Str. 10, 13125 Berlin, Germany*

‡ *Department of Chemistry, Purdue University, 560 Oval Dr., W. Lafayette, IN 47907-2084, USA*

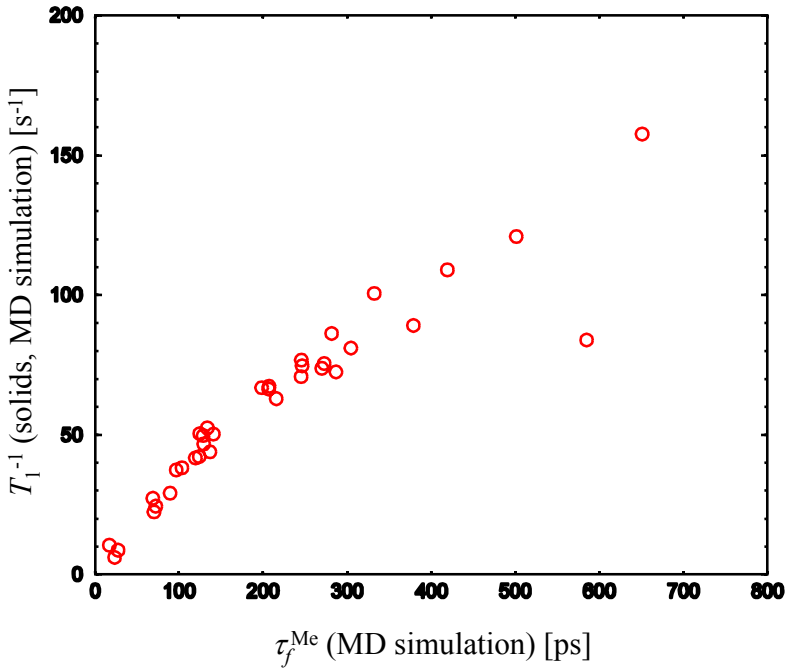

Figure S1. Simulated solid-state methyl ^{2}H T_1^{-1} rates as a function of methyl rotation correlation times, τ_f^{Me}. Based on a 40-ns-long MD trajectory[1] of a 63-residue protein L[2] recorded with the program NAMD.[3] The rates for multiple methyl sites were computed assuming axially symmetric deuterium quadrupolar tensor with the principal axis along the CH bond and the magnitude e^2qQ/h = 167 kHz.[4]

The correlation functions were evaluated as $g(\tau) = (4\pi/5)\sum_{q=-2}^{2} \overline{Y_{2q}(\Omega(t))Y_{2q}^{*}(\Omega(t+\tau))} - \overline{Y_{2q}(\Omega(t))}\,\overline{Y_{2q}^{*}(\Omega(t))}$ and multiplied by the window function, $\exp(-\tau/100\,\mathrm{ns})$, in order to eliminate unreasonably long tails which are not supported by the length of the MD trajectory.

To derive τ_f^{Me} values, we extracted from the MD trajectory the time dependence of the dihedral angle associated with methyl rotation, $\chi(t)$. This dependence was used as an input to generate a correlation function $g^{\mathrm{Me}}(\tau)$ (assuming rigid tetrahedral geometry of the methyl group). The result was then fitted to the expression $g^{Me}(\tau) = (1/9) + (1-(1/9))\exp(-\tau/\tau_f^{\mathrm{Me}})$, thus arriving to the best-fit value of τ_f^{Me} which characterizes the spinning of the methyl group.

It is known that molecular dynamics employing CHARMM force field tends to overestimate τ_f^{Me}.[5, 6] In particular, residues with τ_f^{Me} >500 ps (points on the right side of the plot) suffer from poor sampling of methyl rotation and are generally unreliable. Otherwise, a tight correlation between the simulated T_1^{-1} rates and τ_f^{Me} is obvious in the plot.

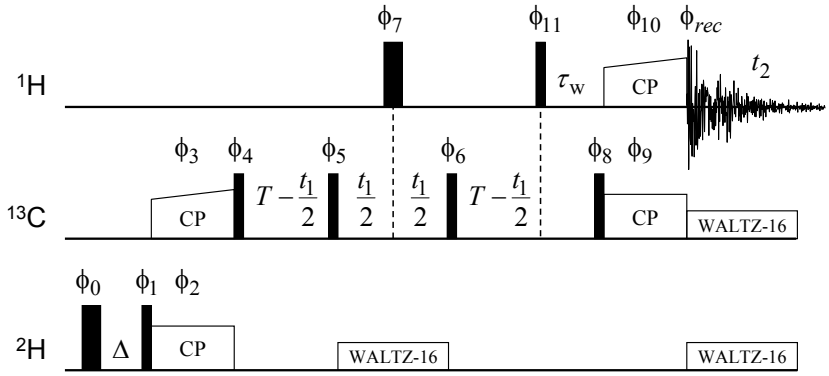

Figure S2. A solid-state NMR experiment for measuring ^{2}H T_1^{-1} relaxation in methyl groups. The sequence was designed for application to the samples that are selectively ^{13}C-labeled in the methyl position and contain both ^{1}H and ^{2}H spins within a given methyl group. Narrow (wide) pulses were applied with a flip angle of 90° (180°). The *rf* carriers were set at 4.94 (HDO line) and 20.8 for ^{1}H and ^{13}C, respectively. The hard pulses were applied with the power levels of 60, 41, and 71 kHz for ^{1}H, ^{13}C, and ^{2}H, respectively. WALTZ-16 decoupling[7] on the ^{13}C and ^{2}H channels employed a 2.5 and 2.8 kHz field, respectively. For the first CP element, the ^{2}H field was 64 kHz and the ^{13}C field was matched at (-1) spinning sideband, with the span of the linear ramp 10 kHz.[8, 9] For the second CP element, the ^{13}C field was 16.5 kHz and the ^{1}H field was matched at (+1) spinning sideband, with the span of the linear ramp 12 kHz. The delays used were: $\tau_{CP}(^2\text{H},^{13}\text{C}) = 4.6$ ms, $\tau_{CP}(^{13}\text{C},^1\text{H}) = 2$ ms, $T = 65$ ms, $\tau_W = 20$ ms, and Δ =[0, 5, 20, 35, 70, 100, 250] ms. The recycling delay between the two consecutive scans was 0.5 s. The spectral widths in the ^{13}C and ^{1}H dimensions were 3100 and 60000 Hz, respectively (the latter was extended to avoid folding of the spinning sidebands in the spectrum). The phase cycle was ϕ0 = y, ϕ1 = (x,-x), ϕ2 = 16(-y)16(y), ϕ3 = 32(x)32(-x), ϕ4 = 32(y)32(-y), ϕ5 = 32(-x)32(x), ϕ6 = x, ϕ7 = (x,-x), ϕ8 = 4(x)4(-x), ϕ9 = y, ϕ10 = 2(x,x,-x,-x)2(y,y,-y,-y), ϕ11 = 16(y)16(x)16(-y)16(-x), ϕrec = P,$\overline{\text{P}}$,$\overline{\text{P}}$,P, where P = (x,-x,-x,x)(-x,x,x,-x)(y,-y,-y,y)(-y,y,y,-y). Quadrature detection in t_1 was achieved by States-TPPI[10] of ϕ6. The sample spinning rate was 24 kHz.

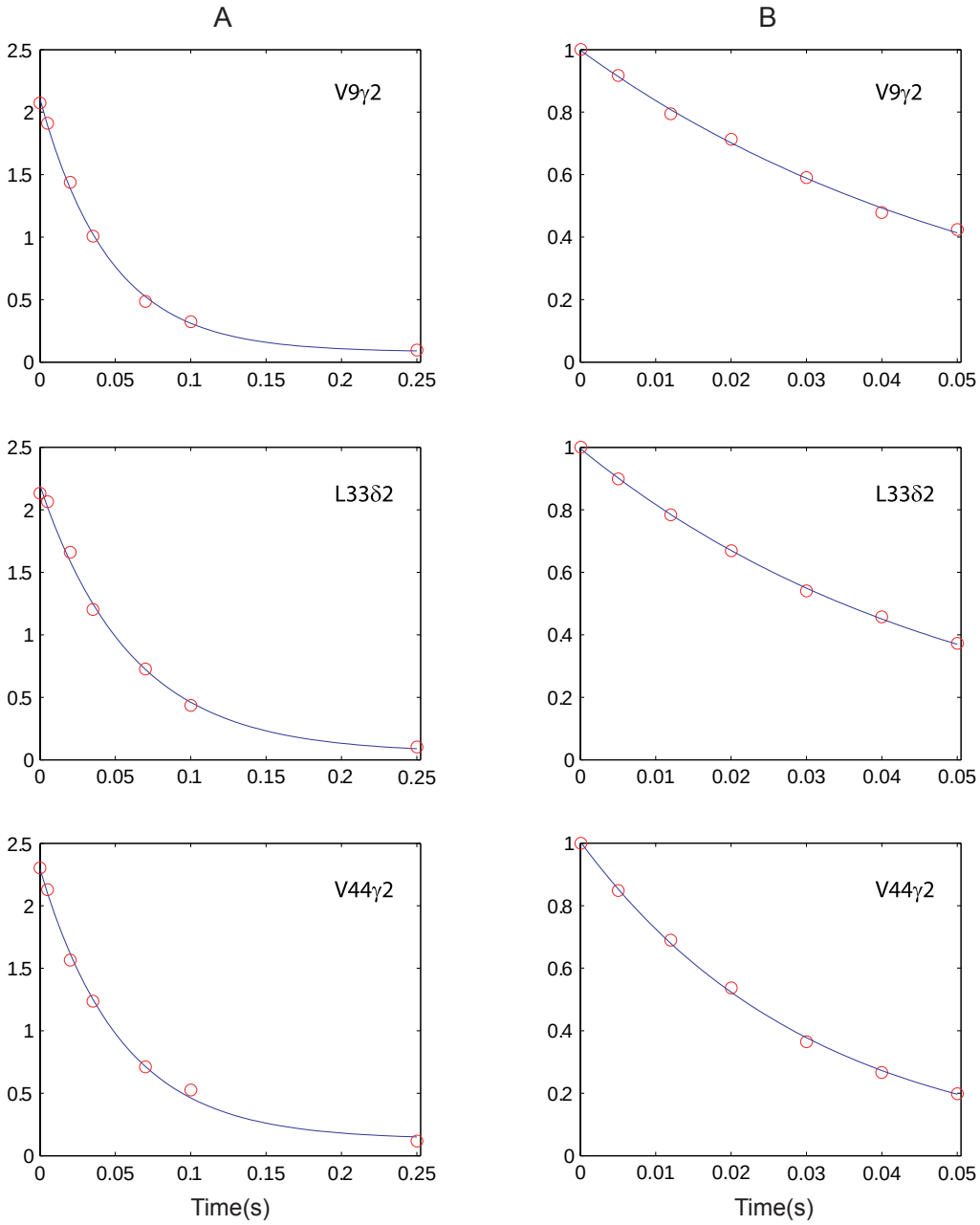

Figure S3. Methyl ^{2}H T_1^{-1} relaxation profiles as recorded in solid (left column) and solution (right column) experiments. The three methyls in this figure illustrate a typical quality of solid-state data (specifically, the data were sorted according to the exponential fitting *rmsd* and three residues were picked from the middle of the list). For comparison, the solution data for these same residues are presented in the right column. The data were recorded in 20 and 60 hours for solution- and solid-state experiments, respectively. All measurements were conducted at 600 MHz, 10 °C (in the case of the solid-state experiments, sample heating has been taken into consideration). The sample conditions for solution-state experiment were 1.5 mM protein, pH 3.5 (unbuffered), 90:10 H_2O:D_2O. For solid studies, the protein was precipitated by means of pH shift as described previously.[11, 12] The peak intensities in the spectra were integrated using nlinLS[13] and fitted according to $(I_0 - I_\infty)\exp(-\Delta / T_1) + I_\infty$ (solid) or $I_0 \exp(-\Delta / T_1)$ (solution).

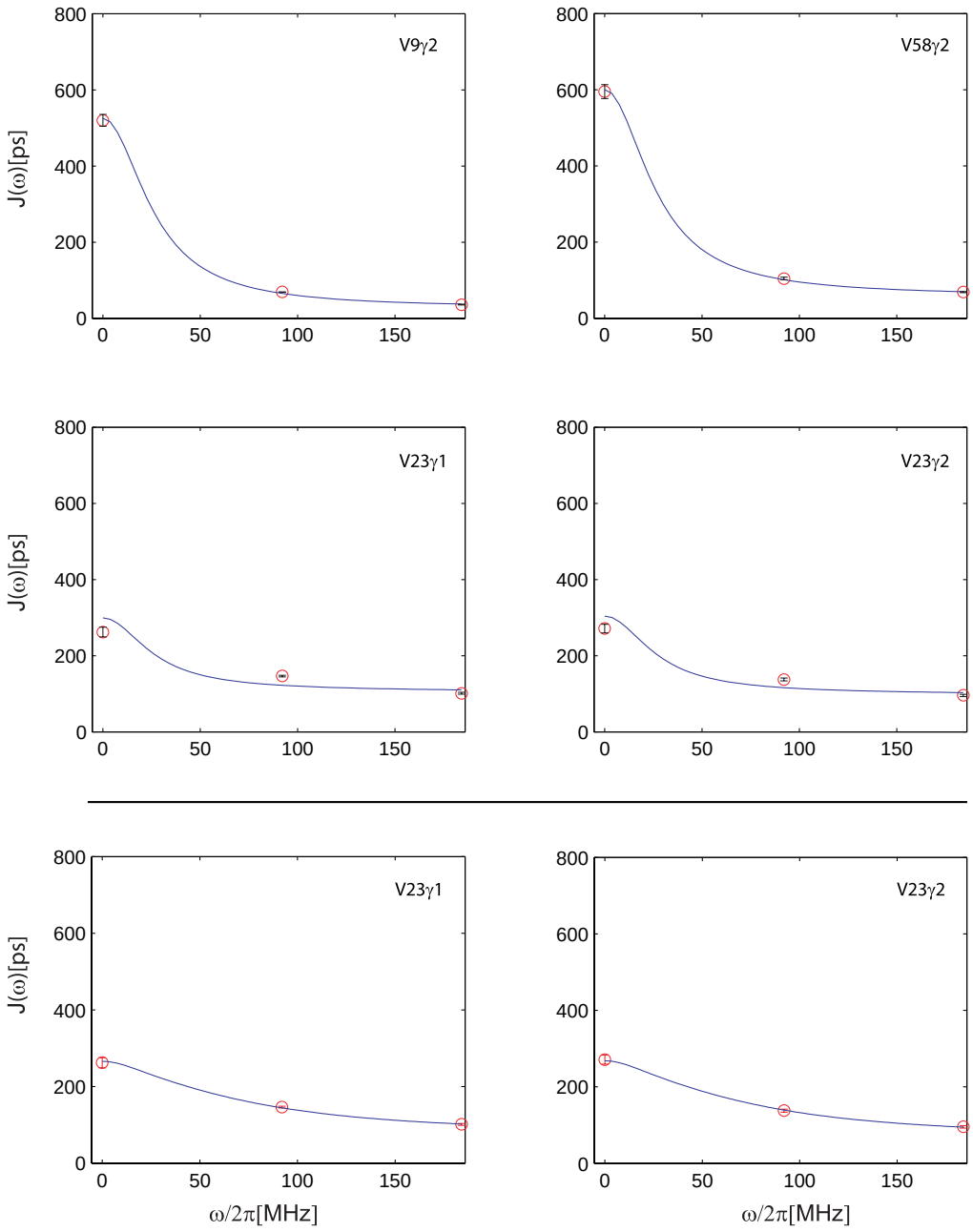

Figure S4. Spectral density mapping for selected methyl sites in the α-spectrin SH3 domain. The three spectral densities, $J(0)$, $J(\omega_D)$, and $J(2\omega_D)$, have been extracted from T_1^{-1}, $T_{1\rho}^{-1}$, and T_{1zz}^{-1} (quadrupolar order) rates measured in solution. The (small) error bars have been generated using the Monte-Carlo procedure. The curves have been generated by fitting T_1^{-1}, $T_{1\rho}^{-1}$, and T_{1zz}^{-1} to Eq. 1 (adapted for anisotropically tumbling molecule). Quadrupolar coupling constants were assumed to be uniform, $e^2qQ/h = 167$ kHz .[4] The top two panels illustrate the typical quality of the fit (specifically, we sorted the data according to the fitting *rmsd* and picked a pair of residues from the middle of the list). The agreement throughout the data set is excellent with the exception of Val-23 (middle row) where the correlation function is affected by rotameric jumps on the time scale of several nanoseconds.

The data from Val-23 were also interpreted using a more sophisticated model (bottom row).

Specifically, the data from both Val-23 methyls (six experimentally measured rates) were fitted to the extended Lipari-Szabo type model.[14, 15] In doing so, fast-motion variables S^2 and τ_f were fitted for each methyl group individually, whereas slow-motion parameters S_s^2 and τ_s were common for both sites. Good fits were obtained in the range of S_s^2 = 0.00 – 0.15, with respective time scales τ_s = 4.0 – 1.7 ns (the curves shown in the bottom portion of the plot correspond to S_s^2 = 0.10, τ_s = 2.8 ns). These results point toward extensive averaging with regard to χ_1. The solid-state T_1^{-1} rates predicted for Val-23 in this analysis were only 1-2 s^{-1} lower than the values obtained on the basis of the simple two-parameter model. Therefore, we choose not to correct the results shown in Fig. 1b.

Methyl group	S^2	τ_f (ps)
A11	0.90 ± 0.03	135 ± 12
A55	0.95 ± 0.04	157 ± 14
A56	0.84 ± 0.02	71 ± 5
V9γ1	0.82 ± 0.03	90 ± 2
V9γ2	0.75 ± 0.03	30 ± 1
V23γ1 [(a)]	0.29 ± 0.03	114 ± 2
V23γ2 [(b)]	0.31 ± 0.02	106 ± 3
V44γ1	0.87 ± 0.04	93 ± 2
V44γ2	0.84 ± 0.01	71 ± 2
V46γ1	0.63 ± 0.02	65 ± 1
V46γ2	0.64 ± 0.01	58 ± 1
V53γ1	0.90 ± 0.04	127 ± 4
V53γ2	0.66 ± 0.03	126 ± 2
V58γ1	0.70 ± 0.03	61 ± 1
V58γ2	0.82 ± 0.03	66 ± 1
I30γ	0.81 ± 0.05	31 ± 3
I30δ	0.30 ± 0.04	35 ± 1
L8δ1	0.62 ± 0.02	27 ± 1
L8δ2	0.71 ± 0.02	49 ± 1
L10δ1	0.70 ± 0.03	9 ± 1
L10δ2	0.61 ± 0.02	47 ± 1
L12δ1	0.69 ± 0.03	27 ± 1
L12δ2	0.72 ± 0.06	54 ± 1
L31δ1	0.29 ± 0.02	89 ± 1
L31δ2	0.34 ± 0.02	43 ± 1
L33δ1	0.66 ± 0.02	34 ± 1
L33δ2	0.79 ± 0.02	34 ± 1
L34δ1	0.62 ± 0.02	47 ± 1
L34δ2	0.62 ± 0.03	54 ± 2
L61δ1	0.45 ± 0.01	33 ± 1
L61δ2	0.43 ± 0.01	41 ± 1

Table S1. Order parameters, S^2, and correlation times, τ_f, obtained from the Lipari-Szabo analysis of methyl ^{2}H T_1^{-1}, $T_{1\rho}^{-1}$, and T_{1zz}^{-1} relaxation data in solution. The data are from the pyruvate-based (selectively ^{13}C-labeled) sample, except in the case of the Ala and Ile-δ sites where the data are from the glucose-based (uniformly ^{13}C-labeled) sample.

(a) The extended analysis, see Fig. S4, yields S^2 = 0.69 – 0.87 and τ_f = 92 – 80 ps

(b) The extended analysis, see Fig. S4, yields S^2 = 0.76 – 0.92 and τ_f = 82 – 69 ps

Effects of ^{2}H-^{2}H spin diffusion on measurements of deuterium T_1^{-1} relaxation rates.

Dipolar-driven spin diffusion in deuterated molecules under MAS conditions was first described by Alla, Eckman, and Pines.[16] These authors also pointed out that spin-diffusion can compromise ^{2}H T_1^{-1} measurements. In brief, the interchange of magnetization between different ^{2}H sites tends to equalize the observable relaxation rates. Notably, partial averaging takes place between rapidly relaxing methyls and the rest of the deuterium spins which relax slowly.

In order to simulate this effect, we took advantage of the formalism developed by Gan and Robyr for the system of two coupled spins I=1, S=1.[17] The starting geometry was that of the aliphatic chain, with spin I representing methyl and spin S representing proximal methine or methylene. For example, in the case of valine side chain the treatment was formulated for $^2H^{\gamma}$ and $^2H^{\beta}$ spins. The quadrupolar tensor for $^2H^{\beta}$ was assumed to be axially symmetric with unique axis along H^{β}-C^{β} bond and the amplitude e^2qQ/h = 167 kHz.[4] For the methyl group, the partially averaged tensor has the symmetry axis along C^{β}-C^{γ} bond and the amplitude $(1/3)e^2qQ/h$ = 55.7 kHz. The quadrupolar relaxation rates were simulated for the methyl group assuming τ_f = 80 ps, $\omega_0^H/2\pi$ = 600 MHz. The chemical shift difference between $^2H^{\gamma}$ and $^2H^{\beta}$ was taken to be 1.17 ppm according to the average value reported in the BMRB database.[18] The sample spinning rate was assumed to be 24 kHz, same as in the experimental study.

The treatment was formulated using the product operator basis. Since none of the terms in the master equation (including the dipolar flip-flop term and quadrupolar relaxation) can induce coupling between ΔM=0, 1, 2, etc. manifolds, only ΔM=0 manifold has been retained to analyze longitudinal relaxation. This manifold is spanned by:

$$\{E, I_z, 3I_z^2 - 2E\} \otimes \{E, S_z, 3S_z^2 - 2E\} \quad \text{(S1.1)}$$

$$\{I_+, I_+I_z + I_zI_+\} \otimes \{S_-, S_-S_z + S_zS_-\} \ + \text{conjugate operators} \quad \text{(S1.2)}$$

$$\{I_+^2\} \otimes \{S_-^2\} \ + \text{conjugate operators} \quad \text{(S1.3)}$$

for the total of 19 operators, including identity. The relaxation rates for these modes, including two-spin modes, can be calculated in a straightforward fashion. In doing so we assumed that methyl spin I is relaxed via the quadrupolar mechanism modulated by methyl rotation. Spin S, on the other hand, represents the 'rigid' deuterium site for which quadrupolar relaxation is known to be inefficient (the rate was set to zero in our simulations).[16] With only one relaxation channel to consider, the set of the quadrupolar relaxation rates for the modes Eq. (S1) is given by familiar expressions. [19]

The dipolar Liovillian matrix was evaluated according to Gan and Robyr in the basis of fictitious spin-1/2 and spin-1 operators.[17] It was subsequently transformed into the basis Eq. (S1). The elements of the matrix connecting S_z and $3S_z^2 - 2E$ with the rest of the modes, $(S_z\hat{\hat{H}}_{dip}B_i)$ and $([3S_z^2 - 2E]\hat{\hat{H}}_{dip}B_i)$, have been multiplied by 3 to account for the presence of three equivalent ^{2}H spins in the methyl group. The Liouvillian matrix was then combined with the relaxation matrix and the spin evolution was computed beginning with the initial conditions $I_z(0) = S_z(0) = 1$, corresponding to the non-selective deuterium relaxation measurement.

The decay curve $I_z(t)$ obtained in this manner is representative of a microcrystal with certain specific orientation relative to the rotor frame. To calculate the response from the powder sample, this calculation has been repeated for 900 different microcrystal orientations which provide optimal sampling of the unit sphere[20] (the convergence of the integration procedure was confirmed by reproducing Fig. 2 in the work by Gan and Robyr[17]). The resulting $I_z(t)$ curves were then added with the prescribed weights[20] and the net decay profile $< I_z(t) >$ was thus generated.

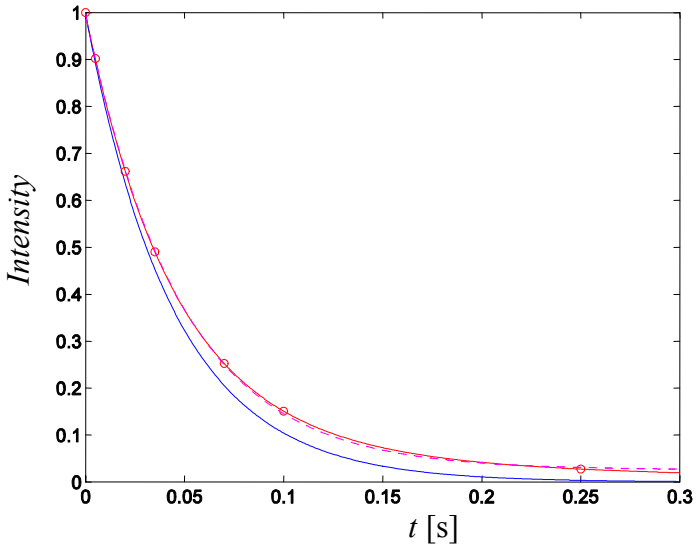

Figure S5. Simulated methyl ^{2}H $< I_z(t) >$ relaxation profiles. Blue curve: $\exp(-T_1^{-1}t)$, where T_1^{-1} is the 'true' $^2H^{\gamma}$ quadrupolar relaxation rate. Red curve: the result of numeric simulations accounting for spin diffusion to $^2H^{\beta}$. Red circles: points from the red curve that sample the same delays as employed in our experimental measurements. Magenta curve (dashed line, closely overlaps with the red curve): single-exponential fit of the points represented by the red circles. The fit, which yields the apparent rate $T_{1,app}^{-1}$, is obtained using the same procedure as is used for the analyses of the experimental data.

The results of this simulation are presented in Fig. S5. As expected, the decay of the methyl magnetization is slowed down due to the spin diffusion involving slowly relaxing $^2H^{\beta}$ (cf. red and blue curves). The apparent methyl rate drops by 6% relative to the target value. Conversely, the simulated decay of $^2H^{\beta}$ (not shown) is entirely due to the presence of the "methyl sink" nearby. The simulated apparent rates, $T_{1,app}^{-1}(^2H_3^{\gamma})$ =21 s^{-1} and $T_{1,app}^{-1}(^2H^{\beta})$ =5 s^{-1}, are in agreement with the recent measurements on u-^{2}H NAc-Val sample performed under similar (although not identical) conditions.[21]

Of note, the effect of ^{2}H-^{2}H spin diffusion is strongly dependent on the chemical shift offset between the two deuterium spins. This effect is illustrated in Fig. S6a. According to conventional wisdom, the dipolar flip-flop term cannot effectively couple two spin states with large energy separation.

As a result, spin diffusion effects disappear if the difference in chemical shifts becomes sufficiently large, >3 ppm. On the other hand, when chemical shifts are degenerate spin diffusion leads to thorough mixing of magnetization. When the mixing occurs between three methyl ^{2}H spins with the relaxation rate T_1^{-1} and a single proximal ^{2}H spin with the relaxation rate 0, the apparent decay rate is $T_{1,app}^{-1} = (3/4)T_1^{-1}$ (*y*-axis intercept in Fig. S6a). An important corollary of this result is that Ala and Thr, that typically show large $\Delta\Omega$, are less likely to be affected by spin diffusion then Leu and Ile.[22]

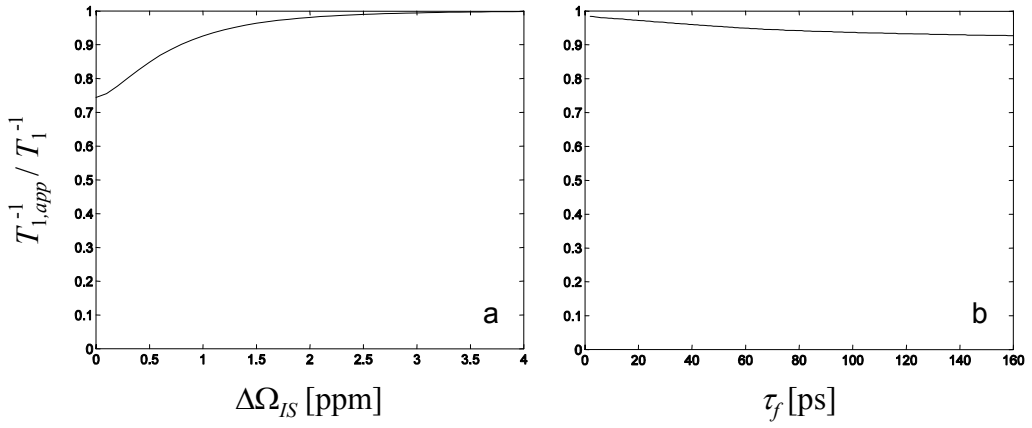

Figure S6. Relative accuracy of the measurable methyl $^2H^\gamma$ T_1^{-1} rate as a function of (a) chemical shift offset between $^2H^\gamma$ and the dipolar-coupled $^2H^\beta$ and (b) fast internal motion correlation time. The graphs have been generated by repeating the calculation Fig. S5 with (a) $\Delta\Omega$ varied, τ_f = 80 ps, and (b) τ_f varied, $\Delta\Omega$ = 1.17 ppm. The single-exponential fitting of the simulated data proved to be practically perfect over the entire range of $\Delta\Omega$, τ_f. Note that the spin dynamics behind these graphs is rather complex: generally speaking, it involves a build-up of a number of spin modes that relax at different rates.

Another instructive dependence is plotted in Fig. S6b. It turns out that methyl sites with long τ_f and, accordingly, with high quadrupolar relaxation rates are more prone to spin-diffusion effects. This effect can be explained in a familiar fashion: broadening of ^{2}H transitions facilitates polarization transfer in the system with a chemical shift offset. This is relevant for the Ala and Val side chains that tend to have higher relaxation rates (cf. Tab. S1).

One additional source of ^{2}H broadening is dipolar interaction with proximal protons. While our glucose-derived samples are uniformly deuterated, pyruvate-derived samples contain protons in methyl positions. A simple way to account for the presence of protons is to add an empirical decay constant to the description of the two-spin deuterium system.[17] Based on the proton linewidth, we estimated this decay constant to be on the order of ca. 15 s^{-1}. This generic number was subsequently added to the auto-relaxation rates of the coherences Eqs. (S1.2, S1.3) and the simulations of Fig. S5 were repeated. The resulting enhancement of the spin diffusion was rather insignificant (additional 1% drop in the

apparent methyl ^{2}H relaxation rate). We note that the role of protons in this context is similar to that in proton-driven ^{13}C-^{13}C spin diffusion.[23]

In addition to the intra-residue processes, we also considered the possibility of spin diffusion between different methyl groups. As a test case, we selected Val53 γ2 and Val58 γ1 that form a very close contact in the structure of the SH3 domain (effective distance after averaging over fast methyl rotations 3.5 Å).[24] The correlation times τ_f for the two respective methyl groups were set to 126 and 61 ps, in accordance to the solution-state data. The chemical shift offset $\Delta\Omega$, as observed in the spectrum, was 0.25 ppm. To account for the presence of three equivalent deuterons in each methyl group, the elements of the dipolar Liouvillian connecting I_z and $3I_z^2 - 2E$ with the rest of the modes were multiplied by 3 (same for the elements connecting S_z and $3S_z^2 - 2E$ with the rest of the modes).

The simulations conducted under these conditions produced the following results. With significantly different τ_f values, the 'true' T_1^{-1} rates for the methyls in question are 27 and 19 s^{-1}. The spin diffusion causes partial averaging of the rates, resulting in $T_{1,app}^{-1}$ of 24.5 and 21.5 s^{-1}. This illustrates the pervasive character of deuterium spin diffusion in the experiments with sample spinning.

As always the case with spin-diffusion, any attempt at a truly quantitative description is predicated on the analysis of a very large spin network. In the context of the present experiment this is clearly not feasible. For each individual ^{2}H spin the outcome will be dependent on the configuration of the surrounding spin network, the corresponding chemical shifts, and the intrinsic relaxation rates. Other factors can also play a role. For example, the initial conditions of the inversion-recovery experiment Fig. S2 are likely to be non-trivial. While ^{2}H magnetization of the methyls is inverted reasonably well with a high-power 180° pulse, only partial inversion can be expected for other ^{2}H sites where e^2qQ/h is not averaged by internal motion. Furthermore, slowly relaxing ^{2}H spins are likely to become partially saturated during the measurement which uses relatively short interscan delays. As already mentioned, one should also consider the effect of proximal protons on ^{2}H-^{2}H spin diffusion. Thus, generally speaking, the problem is highly complex. Nonetheless, the above simplified analysis has demonstrated that the apparent T_1^{-1} relaxation rates for methyl ^{2}H spins tend to be (*i*) lower than expected and (*ii*) more uniform than expected. The deviations from the true T_1^{-1} values are on the order of ≥10%, consistent with our experimental observations.

References

1. Eichmüller, C.; Ryabov, Y.; Skrynnikov, N. R., to be published.
2. Scalley, M. L.; Yi, Q.; Gu, H. D.; McCormack, A.; Yates, J. R.; Baker, D., *Biochemistry* **1997,** 36, (11), 3373-3382.
3. Phillips, J. C.; Braun, R.; Wang, W.; Gumbart, J.; Tajkhorshid, E.; Villa, E.; Chipot, C.; Skeel, R. D.; Kale, L.; Schulten, K., *J. Comput. Chem* **2005,** 26, (16), 1781-1802.
4. Mittermaier, A.; Kay, L. E., *J. Am. Chem. Soc.* **1999,** 121, (45), 10608-10613.
5. Chatfield, D. C.; Szabo, A.; Brooks, B. R., *J. Am. Chem. Soc.* **1998,** 120, (21), 5301-5311.
6. Chatfield, D. C.; Augsten, A.; D'Cunha, C.; Wong, S. E., *J. Comput. Chem* **2003,** 24, (9), 1052-1058.
7. Shaka, A. J.; Keeler, J.; Frenkiel, T.; Freeman, R., *J. Magn. Reson.* **1983,** 52, (2), 335-338.
8. Metz, G.; Wu, X. L.; Smith, S. O., *J. Magn. Reson. Ser. A* **1994,** 110, (2), 219-227.
9. Baldus, M.; Geurts, D. G.; Hediger, S.; Meier, B. H., *J. Magn. Reson. Ser. A* **1996,** 118, (1), 140-144.
10. Marion, D.; Ikura, M.; Tschudin, R.; Bax, A., *J. Magn. Reson.* **1989,** 85, (2), 393-399.
11. Pauli, J.; van Rossum, B.; Förster, H.; de Groot, H. J. M.; Oschkinat, H., *J. Magn. Reson.* **2000,** 143, (2), 411-416.
12. Chevelkov, V.; Rehbein, K.; Diehl, A.; Reif, B., *Angew. Chem. Int. Ed.* **2006,** 45, (23), 3878-3881.
13. Delaglio, F.; Grzesiek, S.; Vuister, G. W.; Zhu, G.; Pfeifer, J.; Bax, A., *J. Biomol. NMR* **1995,** 6, (3), 277-293.
14. Clore, G. M.; Szabo, A.; Bax, A.; Kay, L. E.; Driscoll, P. C.; Gronenborn, A. M., *J. Am. Chem. Soc.* **1990,** 112, (12), 4989-4991.
15. Skrynnikov, N. R.; Millet, O.; Kay, L. E., *J. Am. Chem. Soc.* **2002,** 124, (22), 6449-6460.
16. Alla, M.; Eckman, R.; Pines, A., *Chem. Phys. Lett.* **1980,** 71, (1), 148-151.
17. Gan, Z. H.; Robyr, P., *Mol. Phys.* **1998,** 95, (6), 1143-1152. In Eq. (20) of this paper the matrix element (1,3) should read $\sqrt{2}d_{12}^{(456)}$, the matrix element (3,1) should read $-\sqrt{2}d_{12}^{(456)}$, and the matrix element (6,4) should read $-\sqrt{2}d_{12}^{(456)}$. In Fig. 2 of this paper the amplitude of $< d_{12}^{(456)} >$ should be approximately 2-fold lower than indicated in the plot. These corrections have been kindly confirmed by Dr. Zhehong Gan.
18. Doreleijers, J. F.; Mading, S.; Maziuk, D.; Sojourner, K.; Yin, L.; Zhu, J.; Markley, J. L.; Ulrich, E. L., *J. Biomol. NMR* **2003,** 26, (2), 139-146.
19. Millet, O.; Muhandiram, D. R.; Skrynnikov, N. R.; Kay, L. E., *J. Am. Chem. Soc.* **2002,** 124, (22), 6439-6448.
20. Fliege, J.; Maier, U., *IMA J. Numer. Anal.* **1999,** 19, (2), 317-334.
21. Hologne, M.; Chen, Z. J.; Reif, B., *J. Magn. Reson.* **2006,** 179, (1), 20-28.
22. Cavanagh, J.; Fairbrother, W. J.; Palmer, A. G.; Skelton, N. J., *Protein NMR Spectroscopy. Principles and Practice*. Academic Press Inc.: San Diego, 1996.
23. Ernst, M.; Meier, B. H., Spin diffusion. In *Solid-state NMR of polymers*, Ando, I.; Asakura, T., Eds. Elsevier: 1998; Vol. 84, pp 83-122.
24. Chevelkov, V.; Faelber, K.; Diehl, A.; Heinemann, U.; Oschkinat, H.; Reif, B., *J. Biomol. NMR* **2005,** 31, (4), 295-310.